The magnetic flywheel flow meter: Theoretical and experimental contributions

D. Buchenau, V. Galindo, and S. Eckert

Citation: Applied Physics Letters **104**, 223504 (2014); doi: 10.1063/1.4881330
View online: http://dx.doi.org/10.1063/1.4881330
View Table of Contents: http://scitation.aip.org/content/aip/journal/apl/104/22?ver=pdfcov
Published by the AIP Publishing

The magnetic flywheel flow meter: Theoretical and experimental contributions

D. Buchenau,[a] V. Galindo, and S. Eckert
Helmholtz-Zentrum Dresden-Rossendorf, Institute of Fluid Dynamics, Bautzner Landstraße 400, 01328 Dresden, Germany

(Received 24 January 2014; accepted 19 May 2014; published online 4 June 2014)

The development of contactless flow meters is an important issue for monitoring and controlling of processes in different application fields, like metallurgy, liquid metal casting, or cooling systems for nuclear reactors and transmutation machines. Shercliff described in his book "*The Theory of Electromagnetic Flow Measurement*, Cambridge University Press, 1962" a simple and robust device for contact-less measurements of liquid metal flow rates which is known as magnetic flywheel. The sensor consists of several permanent magnets attached on a rotatable soft iron plate. This arrangement will be placed closely to the liquid metal flow to be measured, so that the field of the permanent magnets penetrates into the fluid volume. The flywheel will be accelerated by a Lorentz force arising from the interaction between the magnetic field and the moving liquid. Steady rotation rates of the flywheel can be taken as a measure for the mean flow rate inside the fluid channel. The present paper provides a detailed theoretical description of the sensor in order to gain a better insight into the functional principle of the magnetic flywheel. Theoretical predictions are confirmed by corresponding laboratory experiments. For that purpose, a laboratory model of such a flow meter was built and tested on a GaInSn-loop under various test conditions.
 [http://dx.doi.org/10.1063/1.4881330]

During the sixties of the last century, Shercliff suggested an electromagnetic flow meter which comprises a rotatable soft iron plate carrying a number of equidistantly spaced magnetic poles with alternating polarity[1] (cf. Fig. 1).

Till this day, Shercliffs electromagnetic flow rate sensor appears to be very attractive for measurements, where highly aggressive and electrically conducting fluids are transported at elevated temperatures.[2–4] The contact-less measurement principle circumvents many problems, such as chemical abrasiveness, interfacial effects, and temperature-dependent boundary effects, which complicate the application of sensors requiring a direct contact to the flow. Another similar contact-less electromagnetic flow meter based on a force measurement has been recently introduced under the name of Lorentz Force Velocimetry (LFV).[5]

The operating principle of the magnetic flywheel is based on the Lorentz force ($\vec{F}_L \propto -\sigma B^2 \vec{v}_0$) resulting from the interaction between the applied magnetic field $\vec{B}$ and the induced eddy currents $\vec{j}$ in the fluid having the electrical conductivity σ and moving with the mean velocity $\vec{v}_0$. The Lorentz force causes a braking effect on the electrically conducting liquid, whereas the flow rate sensor experiences an electromagnetic torque which sets the iron plate into rotation. According to Newtons third law, the induced Lorentz force is balanced by an oppositely directed force F_M, which acts on the respective magnets of the flywheel situated closely to the flow channel

$$\vec{F}_L = -\vec{F}_M = \int_V dr^3 \vec{f}_L = \int_V dr^3 \ \vec{j} \times \vec{B}\,. \qquad (1)$$

The electromagnetic force or torque causing the rotation of the flywheel is only balanced by friction losses of the flywheel bearings. At the end of a specific spin-up time, the flywheel approaches an equilibrium state with a constant rotation rate which is supposed to be proportional to the mass flow rate in the duct. In case of negligibly small friction losses, the

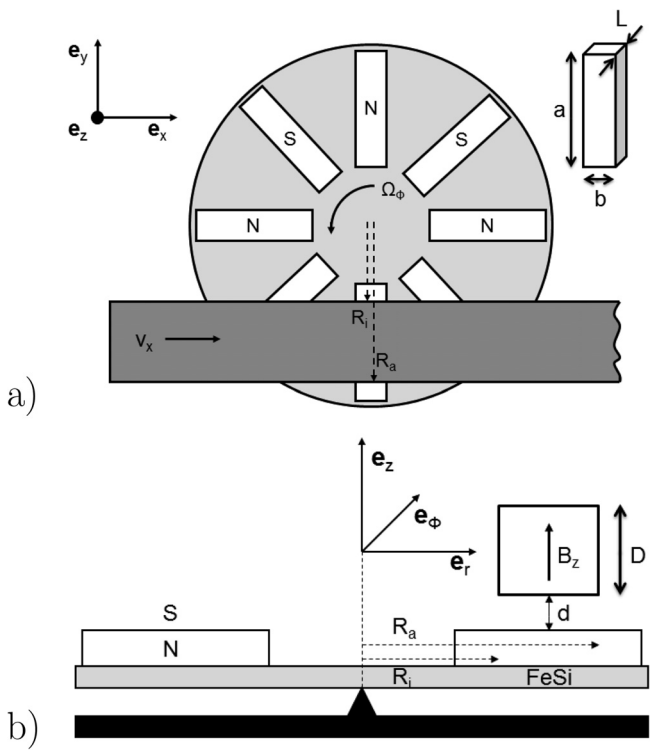

FIG. 1. Top view (a) and lateral view (b) on the magnetic flywheel setup. The permanent magnets exhibit a length *a*, a width *b*, and a depth L aligned with the direction of magnetization.

[a]Electronic mail: d.buchenau@hzdr.de

constant rotation rate depends only on the flow rate and the geometry of the arrangement, while it is independent of the electromagnetic torque itself. A similar characteristic behaviour was shown for the so-called rotating magnet flow meter.[6–8]

The dynamics of the magnetic flywheel can be described by the following equation:

$$J\left(\partial_t + \gamma^{-1}\right)\vec{\Omega} = \int_V dr^3\left(\vec{r}\times\vec{f}_L\right), \tag{2}$$

in which J denotes the moment of inertia of the flywheel, Ω is the rotational frequency, and γ is the frictional decay time. Previous considerations of the magnetic flywheel usually neglected the back reaction of the rotating magnets to the melt flow resulting in an antipodal force $\vec{F}_M \propto \sigma B^2 \vec{v}_\phi$, in which $\vec{v}_\phi$ denotes the mean peripheral speed of the flywheel. However, the comprehension of the antipodal force $\vec{F}_M$ is essential for a complete analysis of the measuring principle. Assuming a constant rotational frequency Ω of the magnetic flywheel, the temporal variation of the magnetic induction in the fluid channel above the flywheel can be described as

$$\vec{B} = \frac{B_r}{\pi}\; G(z)\, \mathrm{e}^{i(\Omega t - N\phi)}\, \vec{e}_z = B_0\, \mathrm{e}^{i(\Omega t - N\phi)}\, \vec{e}_z, \tag{3}$$

where N denotes the number of magnetic pole pairs and ϕ is azimuthal angle in cylindrical coordinates. The remanence of Sm-Co permanent magnets ($B_r = 1.1$ T) stands for the residual magnetization of a material after magnetization. The function $G(z)$ (cf. Eq. (4) and Fig. 2) represents the decay of the magnetic induction as a function of the distance (z) measured from the surface of the magnet (cf. Fig. 1 for the dimensions a, b, and L).

$$G(z) = \arctan\left(\frac{ab}{2z\sqrt{4z^2+a^2+b^2}}\right) - \arctan\left(\frac{ab}{2(L+z)\sqrt{4(L+z)^2+a^2+b^2}}\right). \tag{4}$$

This expression can be derived from the Biot-Savart law.

The governing equation for the calculation of the induced electromagnetic field can be derived from the Maxwell equations. We take into account the Ohm's law for conducting media and obtain the following magnetic field transport equation:

$$\partial_t\vec{B} + (\vec{v}\cdot\nabla)\vec{B} = \frac{1}{\mu_0\sigma}\nabla^2\vec{B} + (\vec{B}\cdot\nabla)\;\vec{v}. \tag{5}$$

The relative velocity between the permanent magnets and the electrically conducting melt can be expressed as: $\vec{v} = \vec{v}_0 + \vec{v}_\phi = (v_0 - \Omega r)\;\vec{e}_\phi$. After substitution of Ampere's law $(\nabla\times\vec{B} = \mu_0\,\vec{j})$ in Eq. (5) and taking into account the expression (3), we obtain the governing equation for the spacial distribution of the electrical current density $\vec{j}$

$$\nabla\times\vec{j} = -i\;\sigma\left\{(N+1)\Omega - N v_0\, r^{-1}\right\}\vec{B}. \tag{6}$$

The Kirchhoff's law for the electric charge conservation $(\nabla\cdot\vec{j} = 0)$ enables the introduction of a stream function

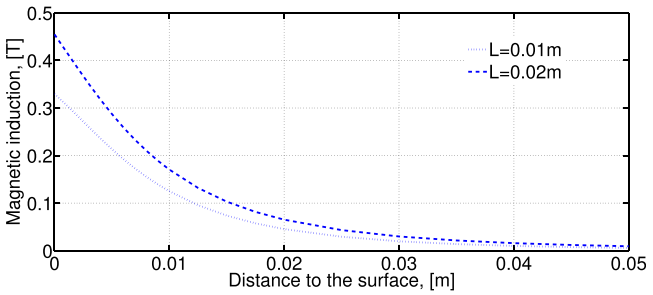

FIG. 2. Magnetic induction as a function of the distance to the surface of the permanent magnets.

$\Psi(r,\phi,t) = f(r)\exp(i(\Omega t - N\phi))$ for the electric current density $\vec{j}$. This stream function provides the angular and radial components of $\vec{j}$ as $j_r = r^{-1}\,\partial_\phi\Psi$ and $j_\phi = -\partial_r\Psi$, respectively. Assuming insulating walls of the flow channel, the amplitude $f(r)$ of the introduced stream function is equal to zero at the radial positions of the fluid boundary R_i and R_a (cf. Fig. 5). Note that only the ϕ-component of $\vec{j}$ contributes to the resulting Lorentz-force density acting on the electrically conductive melt. For a sufficient high number of pole-pairs (N), the final expression for the over one period $T = 2\pi/\Omega$ time averaged Lorentz-force density can be written as

$$\langle\vec{j}\times\vec{B}\rangle_T = -\frac{\sigma B_0^2 N}{2}\left\{\frac{N v_0}{N^2-1} - \frac{\Omega r(N+1)}{N^2-4}\right\}\vec{e}_\phi. \tag{7}$$

The relevant axial component of the torque $M = -c(\phi)D\int_{R_i}^{R_a} dr\; r^2\langle\vec{j}\times\vec{B}\rangle\cdot\vec{e}_z$ acting on the rotatable mounted flywheel can be calculated by an integration of the force density over the whole interaction volume of the magnets with the channel, in which $c(\phi) = \phi - \phi_0$ denotes the sector in which the Lorentz force is induced and D is the thickness of the channel in the z-direction. According to the steady state condition, an equilibrium state can be formulated

$$J\gamma^{-1}\Omega = \frac{D^2 c(\phi)\sigma B_0^2 N}{2}\left\{\frac{N v_0 \bar{R}^2}{N^2-1} - \frac{(N+1)\Omega\bar{R}^3}{N^2-4}\right\}, \tag{8}$$

in which $\bar{R} = (R_i + R_a)/2$ denotes the averaged radius of the flywheel. We consider now the case of vanishing frictional losses $\gamma^{-1} = 0$. Equation (8) can be transformed to

$$v_\phi = \Omega\bar{R} = \left(\frac{N}{N+1}\right)\left(\frac{N^2-4}{N^2-1}\right)\;v_0 = f(N)\;v_0. \tag{9}$$

The conversion of the averaged fluid velocity v_0 into an averaged peripheral speed v_ϕ of the flywheel is given by the function $f(N)$ (cf. Fig. 3), which tends to $\lim_{(N\to\infty)} f(N) = 1$ for a sufficiently large number of pole pairs.

This steady rotation speed of the flywheel is obviously neither dependent on the electrical conductivity of the considered fluid nor on the magnetic induction of the permanent magnets. A certain magnetic induction is nevertheless necessary in order to set the magnetic flywheel into rotation. In reality, the frictional decay rate is not equal to zero, $\gamma^{-1} \neq 0$. Then, Eq. (8) leads to an expression which contains the electrical conductivity of the melt as well as the z-dependent magnetic induction of the permanent magnets (cf. Eq. (10))

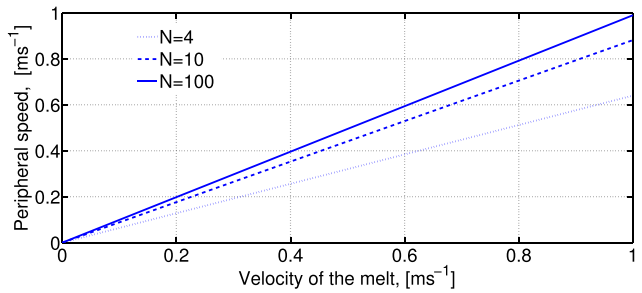

FIG. 3. Dependence of the peripheral speed (v_ϕ) on the number of magnetic pole pairs (N) and the averaged velocity of the melt (v_0) according to Eq. (9) for $\gamma^{-1} = 0$.

$$v_\phi\left(\frac{\alpha}{K_1}+1\right) = f(N)v_0. \tag{10}$$

The influences of the electrical conductivity and the magnetic field strength are included into the correction factor $K_1 = \left(\frac{c(\phi)D^2\sigma\bar{B}^2\bar{R}^3}{2J}\right)\left(\frac{N(N+1)}{N^2-4}\right)$. Furthermore, α denominates the ratio of the frictional decay rate γ^{-1} to the sector of interaction $c(\phi)$. The magnetic induction is approximated by an averaged magnitude $\bar{B} = \frac{1}{D}\int_{z_1}^{z_2} B_0\, dz$, in which z_2 and z_1 denote the distances to the flow channel resulting in the thickness of the channel $D = z_2 - z_1$. Because of this z-dependence of $\bar{B}$, the steady rotation rate of the flywheel decreases at a given flow rate with growing distance between the flywheel and the flow channel.

The transient behavior of the flywheel can be obtained from the solution of the equation of motion (cf. Eq. (2))

$$\Omega(t) = \Omega_0\{1 - e^{-(\alpha+K_1)t}\}, \tag{11}$$

in which Ω_0 can be expressed by the following relation: $\Omega_0 = f(N)v_0 K_1\left(\bar{R}(\alpha+K_1)\right)^{-1}$.

A laboratory model of the magnetic flywheel was manufactured using a soft iron plate with a diameter of 124 mm and a thickness of 5.5 mm. Large-dimensioned Sm-Co magnets ($30 \times 20 \times 10\,\text{mm}^3$) are used in order to provide a high magnetic induction of $B_S = 0.33\,\text{T}$ at the surface. Related to the center of the soft iron plate two layers of permanent magnets are placed with the long edge on the periphery of the plate, i.e., $R_i = 32\,\text{mm}$ and $R_a = 62\,\text{mm}$ (see also Fig. 1).

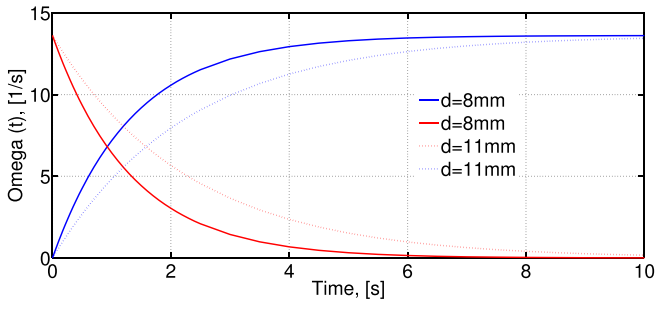

FIG. 4. Time dependence of the angular frequency for different distances d under the assumption of an almost negligible frictional decay rate ($\gamma^{-1} = 0.01\,\text{s}^{-1}$). The solid and exponentially rising and falling graph describing the start-up and run out behavior of the flywheel for an adjusted distance of $d = 8\,\text{mm}$ between the magnets and the channel. The dashed lines are associated with a distance of $d = 11\,\text{mm}$.

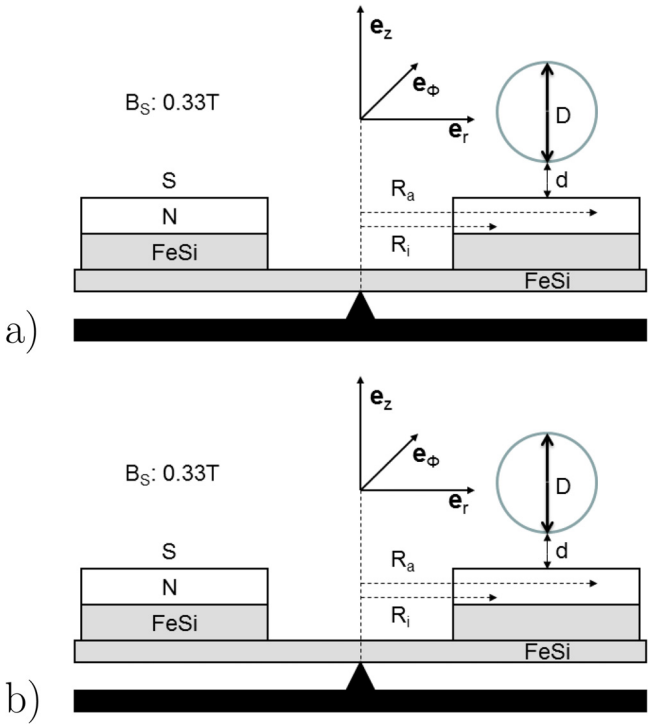

FIG. 5. Schematic diagram of the magnetic flywheel measurements of the equilibrium rotation rate dependent on the surface induction of the magnets and the distance between magnet surface and outer pipe wall ($B_S = 0.33\,\text{T}$ (a) and $B_S = 0.46\,\text{T}$ (b)).

The number of magnetic pole pairs is $N = 4$. The flywheel was installed at a GaInSn flow through an insulating pipe having an inner diameter of $D = 27\,\text{mm}$. For this configuration, a frictional decay rate of $\gamma^{-1} = 0.01\,\text{s}^{-1}$ was experimentally determined in case of low rotational frequencies. Figure 4 illustrates the transient behavior of this flywheel configuration calculated by Eq. (11). The diagram shows the start-up behavior of the flywheel for a fully developed GaInSn channel flow with a mean velocity of $v_0 = 1\,\text{ms}^{-1}$ for two distances d between the flywheel and the channel. The run-out behavior is calculated based on the assumption that the flow can be stopped immediately. The mathematical model (cf. Eq. (9)) predicts for the frictionless case ($\gamma^{-1} = 0$) identical rotation rates for different effective magnetic inductions within the measurement volume at constant distances d to the pipe. To prove this assumption in the experiment, the bottom layer of permanent magnets on the iron plate was substituted by soft iron bars (cf. Fig. 5).

The two-layer arrangement of permanent magnets results in a surface induction of $B_S = 0.46\,\text{T}$. A combination of permanent magnets in the upper layer and soft iron bars in the second layer results in $B_S = 0.33\,\text{T}$. The experimental results presented in Fig. 6 demonstrate that in this case the equilibrium rotation rate of the magnetic flywheel does not depend on the amplitude of the magnetic induction at the surface of the permanent magnets.

Another experiment has been carried out for comparing the equilibrium rotation rates of the flywheel determined at two different distances d. Fig. 7 reveals a slight deviation between the two measured curves. Due to the fact that the frictional decay rate of the laboratory model is close to zero $\gamma^{-1} = 0.01\,\text{s}^{-1}$, this difference is not dramatic, but

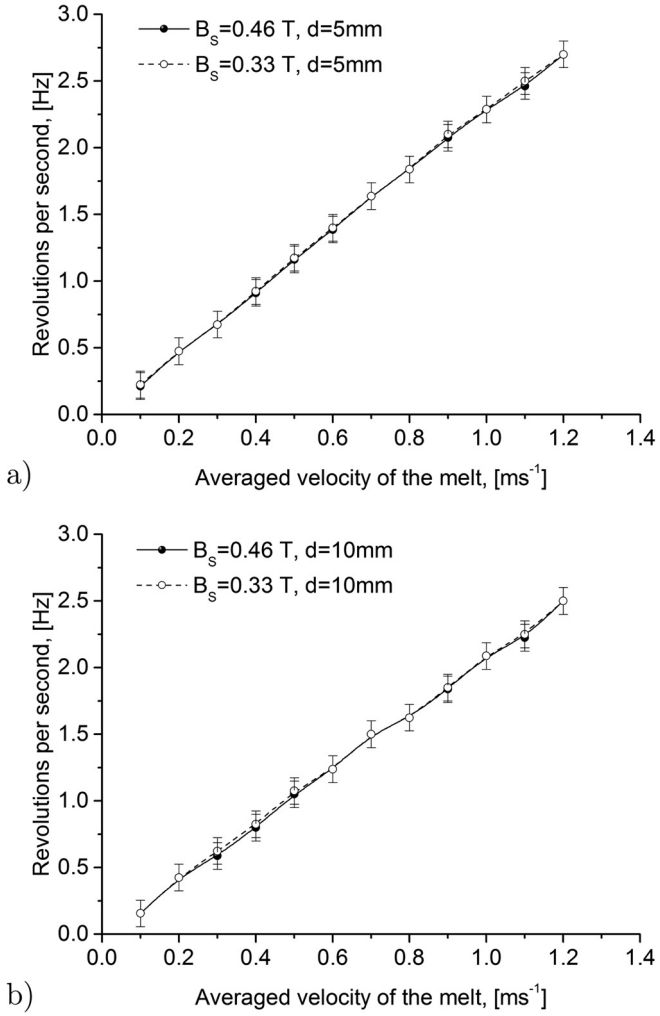

FIG. 6. Measurements of the equilibrium rotation rate on an insulating pipe of the GaInSn loop dependent on the surface induction of the magnets and the distance d.

perceivable. Obviously, the drop of the magnetic field strength with growing distance d has a larger impact on mean magnetic induction $\bar{B}$ as the modification of the surface induction B_S.

A curve resulting from corresponding numerical simulation is also plotted in Fig. 7. The numerical predictions differ from the experimental findings. The deviation might be caused by the assumptions about the distribution of the magnetic induction field along the perimeter which was considered as harmonic in our model. In reality, the distribution of the magnetic induction field has to be described as a step function according to the spatial arrangement of the particular permanent magnets.

In conclusion, the magnetic flywheel can be considered as a reliably and stably operating flow meter. An attractive feature is the absence of any mechanical or electrical contact

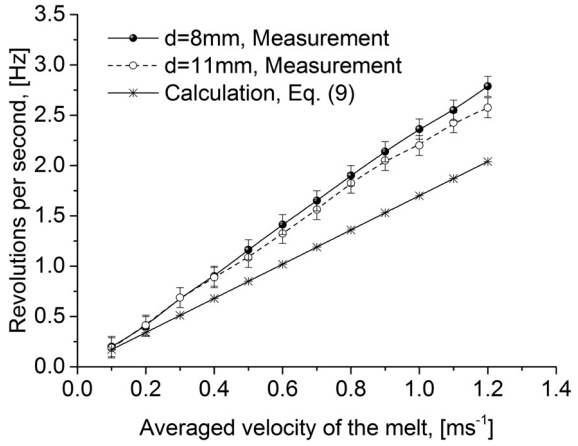

FIG. 7. Rotation rates of the flywheel as a function of the mean GaInSn-flow rate in a pipe with insulating walls for different distances between the permanent magnets and the pipe.

to the flow to be measured. We have shown here that the flow rate measurements of the magnetic flywheel become independent of the electrical conductivity of the liquid metal in the limiting case of vanishing frictional losses. Thus, the equilibrium rotation rate is a function only of the averaged velocity of the melt and the geometry of the set-up. A laboratory model of a magnetic flywheel flow meter was designed, manufactured and tested at a GaInSn-loop with electrically non-conducting pipe walls. The mechanical construction and arrangement of the flywheel have a large impact on the efficiency. Especially, a low-friction bearing is favorable for the reasons mentioned above. Moreover, a compact design with a low mass results in a low moment of inertia and would enable measurements of transient processes with a reasonable temporal resolution.

[1]J. A. Shercliff, *The Theory of Electromagnetic Flow Measurement* (Cambridge University Press, 1962).
[2]V. E. Zirkunov, B. D. Scheigur, G. J. Schermons, and R. K. Kalnins, *Kontaktlose Kontrolle von Flüssigmetallströmungen* (Zinatne, Riga, Latvia, 1973), pp. 49–51.
[3]I. Bucenieks, in *Proceedings of Fifth International Symposium of Magnetic Suspension Technology, Dresden, Germany* (2005), pp. 204–208.
[4]I. Bucenieks, "Perspectives of using rotating permanent magnets for electromagnetic induction pump design," Magnetohydrodynamics **36**, 181–187 (2000).
[5]A. Thess, E. V. Votyakov, and Y. Kolesnikov, "Lorentz force velocimetry," Phys. Rev. Lett. **96**, 164501 (2006).
[6]J. Priede, D. Buchenau, and G. Gerbeth, "Force-free and contactless sensor for electromagnetic flowrate measurements," Magnetohydrodynamics **45**, 451–458 (2009).
[7]J. Priede, D. Buchenau, and G. Gerbeth, "Single-magnet rotary flow meter for liquid metals," J. Appl. Phys. **110**, 034512 (2011).
[8]D. Buchenau, S. Eckert, G. Gerbeth, R. Stieglitz, and M. Dierckx, "Measurement techniques for LBE flows," J. Nucl. Mater. **415**, 396–403 (2011).